Contents list available at CBIORE journal website

International Journal of Renewable Energy Development

Journal homepage: https://ijred.cbiore.id

Research Article

Investigation of a PCM-based latent heat storage system combined with an adiabatic compressed air energy storage system in a renewable energy context

Tony Karam[a,b*], Chantal Maatouk[b], Elias Al Sarraf[a,c]

[a]*Lebanese International University, School of Engineering, Mouseitbeh - PO Box: 146404, Mazraa, Beirut, Lebanon*

[b]*Saint Joseph University of Beirut, Faculty of Engineering, ESIB, P.O. Box 1514 – Riad El Solh, Beirut 1107 2050, Lebanon*

[c]*Lebanese University, Faculty of Engineering, P.O. Box 6573/14 – Badaro, Museum, Beirut, Lebanon*

Abstract. The intermittent nature of renewables has increased the reliance on energy storage technologies to boost the efficiency and stability of power systems. Adiabatic Compressed Air Energy Storage (A-CAES) systems, which recover and reuse the heat generated during compression, have attracted significant attention in recent years. While A-CAES combined with thermal energy storage (TES) systems show promising potential, especially in renewable-integrated power systems, their commercial implementation remains limited, with only a few A-CAES power plants operating and which rely solely on sensible heat storage. The relatively low energy density of sensible heat storage opens the door to exploring latent heat storage (LHS) systems using Phase Change Materials (PCM's), which could play a significant role in enhancing the performance of A-CAES systems. Although high-temperature PCM's have demonstrated efficiency benefits in concentrated solar plants and energy-intensive industries, their integration into A-CAES systems requires further exploration. Accordingly, this paper aimed at simulating and assessing the performance of a combined A-CAES and PCM-based LHS system coupled to a gas turbine and an air turbine, alongside a wind farm. The simulations were conducted for charging durations ranging between 2 and 10 hours, with a fixed 2-hour discharge operation. The resulting fuel-saving efficiency in the gas turbine configuration improved with extended charging durations, ranging between 63.8 % and 66.1%. Furthermore, the exergetic roundtrip efficiency remains higher in the gas turbine configuration for charging durations shorter than 7 hours. Beyond this threshold, however, the air turbine configuration becomes more appealing when the combined CAES–LHS systems are coupled to it, exhibiting higher exergetic roundtrip performance under extended charging conditions. These findings, although theoretical in nature, could serve as a starting point for estimating the performance of the combined CAES-LHS systems and promoting their deployment into power generation applications in a renewable energy context.

Keywords: Wind Farm, Phase Change Materials, Adiabatic Compressed Air Energy Storage, Fuel-Saving Efficiency, Exergetic Roundtrip Efficiency

Received: 17th Nov 2025; Revised: 17th January 2026; Accepted: 4th February 2026; Available online: 15th February 2026

1. Introduction

The global electricity production based on renewable energy sources has witnessed a sharp increase in recent years. According to the International Renewable Energy Agency (IRENA), 585 GW of renewable power capacity were added in 2024, accounting for over 90% of total power expansion globally (International Renewable Energy Agency, 2025). However, the inability to directly control the output of solar and wind energy sources due to their intermittent nature, has led to a heavy reliance on energy storage technologies to boost the efficiency of energy systems while increasing their stability and flexibility. Among these various energy storage technologies, Compressed Air Energy Storage (CAES) has attracted significant attention in numerous research efforts, for various considerations. The lifetime of a CAES system could reach up to 3 times longer than that of the currently dominating Li-ion batteries in terms of charge/discharge cycles (REN21, 2024). It is expected that by 2030, the energy installation costs for CAES will drop down to 44 USD/kWh versus 254 USD/kWh for Li-ion batteries (International Renewable Energy Agency (IRENA), 2017). Moreover, CAES technology was featured as a "proven, economical solution for long duration energy storage" during the 28th meeting of the Conference of the Parties (COP 28), part of the 2023 United Nations Climate Change Conference in Dubai (UAE) (COP28 UAE, 2023). Adiabatic Compressed Air Energy Storage (A-CAES) systems have emerged as a particularly promising CAES configuration in recent years. In an A-CAES system, the compression heat is captured and stored in a dedicated storage, separate from the compressed air reservoir. This stored heat is then reused to reheat the compressed air as it is released from its reservoir.

The theoretical roundtrip efficiency of A-CAES systems is estimated to be in the range of 60%-80% (Zhang *et al.*, 2024). The appealing potential of the adiabatic process for reusing the heat of compression made the A-CAES become the center of interest in power system applications. The integration of A-CAES into a gas-steam combined cycle plant was investigated, whereby the compressed air released from the CAES is

* Corresponding author
Email: tony.karam3@usj.edu.lb (T.Karam)

https://doi.org/10.61435/ijred.2026.61995
ISSN: 2252-4940/© 2026.The Author(s). Published by CBIORE

preheated by the gas turbine exhaust before being fed into an air turbine to produce electrical power (Salvini, 2018). The study concluded that despite the higher investment costs, the proposed CAES system remains highly appealing owing to the technological maturity of the various CAES plant components (such as compressors and expanders), the longer life duration and cheaper plant cost, when compared to Li-ion battery energy storage systems. A CAES system combined with a packed bed unit and electrical heater was proposed in an electric power generation context for the purpose of increasing the capacity factor of the power system without the need to enlarge the compressed air storage size or storage pressure (P. Wang *et al.*, 2019).

Although there are many references in the literature addressing the promising benefits of using thermal energy storage (TES) technologies for the recovery of compression heat in CAES systems, there are much less utility scale applications of combining TES with A-CAES systems for electricity generation. Large-scale Adiabatic CAES systems are still in the process of demonstration and have not yet evolved into full-fledged commercially available technologies (European Association for Storage of Energy (EASE), 2016), for many reasons. First, geographical constraints remain the key weakness associated with large-scale CAES systems which require suitable geological formations or underground caverns for air storage, thereby confining their deployment to specific locations. In fact, the storage of high-pressure air requires very large volumes, particularly when implemented as an artificial above-ground storage facility. This results in a substantially larger physical footprint compared to systems utilizing natural underground caverns. The investment cost of the plant is dominated by the cost of the artificial storage and increases significantly with the increase in the pressure difference between the discharge throttling setpoint and the reservoir pressure at the beginning of the charging phase (Salvini, 2018). Nevertheless, above-ground storage systems are a convenient choice for micro and small-scale CAES systems (Burian & Dančová, 2023).

There are also technical challenges associated with the high-temperature requirements for TES systems and compressors, which stand in the way of their commercialization in the near future (Zhou *et al.*, 2019). On the financial level, other electricity storage technologies are still attracting greater investment, which is standing in the way of the A-CAES deployment at a broader scale (International Renewable Energy Agency (IRENA), 2017). For example, a 200-MW capacity A-CAES plant (the ADELE project in Germany) with 1-GWh storage capacity was put on hold in 2017 due to unforeseen business conditions (Rabi *et al.*, 2023). A 5-MW A-CAES prototype funded by the European Union through the RICAS2020 project (RICAS, 2020) was never built due to outstanding funding (Peter Reinke, 2024). Also, a 5-MW A-CAES facility at the Angas Zinc Mine near Strathalbyn (South Australia) was supposed to be operational in 2020, but the project was ditched mainly for capital expenditure costs (Bloch, 2021).

There are only a few commercial A-CAES power plants currently in operation, as documented in the literature and online news sources. A 300-MW A-CAES power plant constructed in Feicheng City (China) went online in 2024. The plant has a storage capacity of 1,800 MWh and is capable of powering between 200,000 and 300,000 local homes during peak periods. An underground salt cavern with more than 500,000 m3 of storage capacity is used for storing the produced compressed air. The facility is expected to reduce carbon dioxide emissions by approximately 490,000 tons per year (Murray, 2024). Another 100-MW A-CAES power plant at Zhangbei City (China) having approximately 70% roundtrip efficiency was reported to be under commissioning in (Zhang *et al.*, 2024). The plant went online in October 2022 (Shaw, 2024). A 10-MW A-CAES plant in Feicheng City (China) was connected to the power grid in 2021 (Zhang *et al.*, 2024). A 1.75-MW Goderich A-CAES facility in Ontario (Canada) became active in 2019 (Hydrostor, 2024).

Besides these commercial A-CAES installations, small-scale A-CAES prototypes also exist. A 500-kW pilot facility was constructed in China in 2014 for demonstration purposes (S. Wang *et al.*, 2016). A 10-MW A-CAES system was commissioned in 2016 in Bijie City (China) for the purpose of conducting research on wide-load compressors and high-load turbines (Jafarizadeh *et al.*, 2020), and a 1-MW A-CAES prototype was built in 2016 in the Swiss Alps by ALACAES company where a sensible TES (Geissbühler *et al.*, 2018) and a combined sensible/latent TES (Becattini *et al.*, 2018) were tested.

It is worth noting that in all the aforementioned A-CAES installations (except the 1-MW prototype in the Swiss Alps), the compressed air released from the storage system is preheated through sensible heat transfer under various setups: either using fuel burners or a packed bed of rocks or through heat exchange with combustion exhaust gases or a circulating heat transfer fluid (HTF). In view of this reliance on sensible heat transfer, it becomes interesting to shed light on another trending form of energy storage technology, Latent Heat Storage (LHS) systems which make use of Phase Change Materials (PCM's). These systems can be a reliable medium for heat storage and recovery due to their high energy density and constant phase transition temperature over extended periods of time (Mofijur *et al.*, 2019). Despite the promising capabilities of PCM-based thermal energy storage systems, their practical integration into power generation applications has not yet become widespread. In this regard, many studies were undertaken in order to promote the technical feasibility of PCM storage implementation in power systems, especially when integrated with wind and concentrated solar plants (CSP's).

The use of a PCM-based LHS system in a CSP was assessed by Prieto *et al.* (Prieto & Cabeza, 2019). The study confirms that the cheaper and more efficient PCM's are expected to perform similarly to the molten salts that are conventionally used in solar plants. Moreover, the integration of high-temperature PCM-based shell-and-tube heat exchangers (STHE) with concentrated solar power plants appears to be a promising technology since it can help provide stable, continuous and dispatchable electricity output (Q. Li *et al.*, 2019). Optimized designs for high-temperature PCM-based STHE's used in CSP's showed that this latent heat exchanger configuration, if further developed, could compete with the conventional sensible storage systems (Tehrani *et al.*, 2016). Furthermore, next generation CSP's should aim for operating temperatures above 700°C in order to enhance energy density and overall system efficiency (Khan *et al.*, 2022). Exploring the potential benefits of high-temperature PCM-based heat storage systems can be quite promising. Waste heat from energy-intensive industries (EII's) could be stored and recovered in high-temperature PCM-based LHS systems, instead of being wasted or released to the environment. It is estimated that 45% to 85% of the industrial waste heat can be recovered in the latent thermal energy storage systems using inorganic PCM's that are ideal for high-temperature applications (Tawalbeh *et al.*, 2023). Various studies were conducted in order to investigate the

benefits that high-temperature PCM's could offer to the EII's. A composite PCM consisting of a eutectic molten salt mixture called Solar salt (generally used in CSP's) and red mud (an industrial waste of the aluminum industry) was created and tested (Anagnostopoulos *et al.*, 2021). The experimental results showed that the thermal properties and energy density of the new composite PCM make it a suitable candidate for use in high-temperature Latent TES systems for waste heat recovery. A simulation was conducted to analyze the heat exchange in a STHE through which an air stream is preheated (from an initial temperature of 650°C) before entering a ceramic furnace. The STHE incorporates an inorganic PCM with a melting temperature of 885°C, which is charged using the furnace's exhaust gases at temperatures exceeding 1100°C (Royo *et al.*, 2019). The simulation results showed that the air stream exiting the STHE could reach temperatures as high as 865°C leading to a reduction in the natural gas consumption by the furnace, equivalent to saving approximately 570 MWh on a yearly basis. The utilization and conversion of industrial waste heat was also investigated by simulating the integration of a cascaded LHS system with a 420-MW combined-cycle gas turbine power plant (Li *et al.*, 2019). The study demonstrated that despite the relatively large volume of the thermal storage system, this integration is technically feasible for the flexible operation of the power plant.

Based on the literature review presented so far, combining the use of A-CAES and high-temperature PCM-LHS systems appears to have great potential in power generation applications: the PCM's could be used to store the heat generated during air compression and then release it to reheat the compressed air before it expands in a power turbine. As previously noted, the heat exchange between compressed air and TES systems occurred via sensible heat transfer. Moreover, most of the research conducted on latent PCM-based TES systems focused on their integration into either CSP's or EII's only, without the presence of A-CAES systems. To date, only very few studies addressing the A-CAES and PCM-LHS combination in power systems were found in the published literature:

Li *et al.* developed an off-design performance model of a Combined Cooling Heating and Power plant incorporating an A-CAES system and a cascaded PCM-based TES (R. Li *et al.*, 2019). The results of the study showed that a roundtrip efficiency of 96.56% and an electricity efficiency of 61.15% can be achieved. Ghorbani *et al.* proposed an A-CAES system integrated with a multi-stage PCM-based TES and a wind farm in order to produce electric power (Ghorbani *et al.*, 2020). The study reported an expected overall roundtrip efficiency in the range of 70%. Although both studies (R. Li *et al.*, 2019) and (Ghorbani *et al.*, 2020) incorporated a PCM-based latent thermal storage system into an A-CAES facility, sensible heat exchange occurred between the compressed air stream and a HTF (water or thermal oil) during the charging and discharging modes, which implies an inferior heat recovery effectiveness when compared to latent heat exchange.

In another study, Li *et al.* (2021) investigated the coupling of a packed bed filled with PCM capsules to an A-CAES. The results of the thermodynamic model proposed in the study indicated that incorporating two cascaded PCM's would increase the power plant's overall roundtrip efficiency by 4.7% compared to utilizing only one PCM. However, the PCM's used in the packed bed had low-melting temperatures (280 K and 340 K), which makes them inadequate for power cycles that require much higher temperature levels. Mousavi *et al.* explored a novel A-CAES system encompassing cascaded packed bed thermal storage systems filled with encapsulated PCM's in addition to a high-temperature sensible thermal storage (Bashiri Mousavi *et al.*, 2021). The thermo-economic analysis of the overall system revealed a roundtrip energy efficiency of 61.5% and a payback period of 3.5 years. However, the integration of the A-CAES and PCM-based packed bed systems proposed in this study was demonstrated for a small-scale electric power system with a turbine output of 1.1 MW only. This underscores the need to exploit the potential of the A-CAES and PCM-LHS combination at a larger scale.

Becattini *et al.* reported results from the world's first pilot-scale A-CAES plant built in the Swiss Alps, in which an existing packed bed thermocline sensible heat storage system was complemented with a latent heat storage system consisting of an Al–Cu–Si alloy PCM encapsulated in 296 stainless steel tubes (Becattini *et al.*, 2018). The study experimentally showed that the drop in air temperature with time, which would normally occur at the outlet of the sensible heat storage system during discharge operations, was effectively reduced when the PCM-based latent heat storage system was added.

As can be inferred from the above review, the use of high-temperature PCM-based thermal storage systems for exchanging heat with compressed air streams in utility-scale A-CAES power plants is still not quite extensively explored in technical publications. It is also evident that the dynamic performance of LHS systems where direct heat exchange occurs between the PCM and compressed air, without resorting to an intermediate circulating HTF, remains to be further explored. Consequently, there appears to be limited research regarding the integration of A-CAES systems with PCM-based LHS systems. This could indicate an opportunity for further investigation of the benefits and challenges of such integration. Therefore, this paper was centered on simulating and evaluating the performance of a combined A-CAES and high-temperature PCM-LHS, coupled to a utility-scale turbine generator in the presence of a renewable energy source. The outcome of this study helps promote the development of A-CAES demonstration projects that harness the potential benefits from high-temperature PCM's in power generation applications.

2. Methodology

A STHE was adopted for the PCM-based LHS system, for being a promising storage configuration in power plants, as can be construed from the presented literature review. The STHE has compressed air flowing in the shell, and a PCM stored in the tubes.

2.1 System Configurations

The combined A-CAES and PCM-based LHS systems is coupled to either a gas turbine (GT) or an air turbine (AT) in the presence of a wind farm, for the purpose of assessing their performance and impact on the overall system, under various scenarios. An auxiliary compressor (C2) is employed to fill the CAES reservoir using either excess off-peak grid electricity or renewable energy from the wind farm. The showcased system is depicted in the block diagram of Figure 1. It consists of a 14.3-MW Siemens gas turbine (Model no. SGT-400) (Siemens Energy, 2025) coupled to the combined A-CAES and PCM-LHS systems, alongside a wind farm. The gas turbine's exhaust heat recovery system (EHR) is represented by a plate-fin regenerator.

In Mode M1 (standalone mode), the gas turbine operates using its own compressor (C1) without engaging any of the energy storage systems. In Mode M2 (Discharge mode),

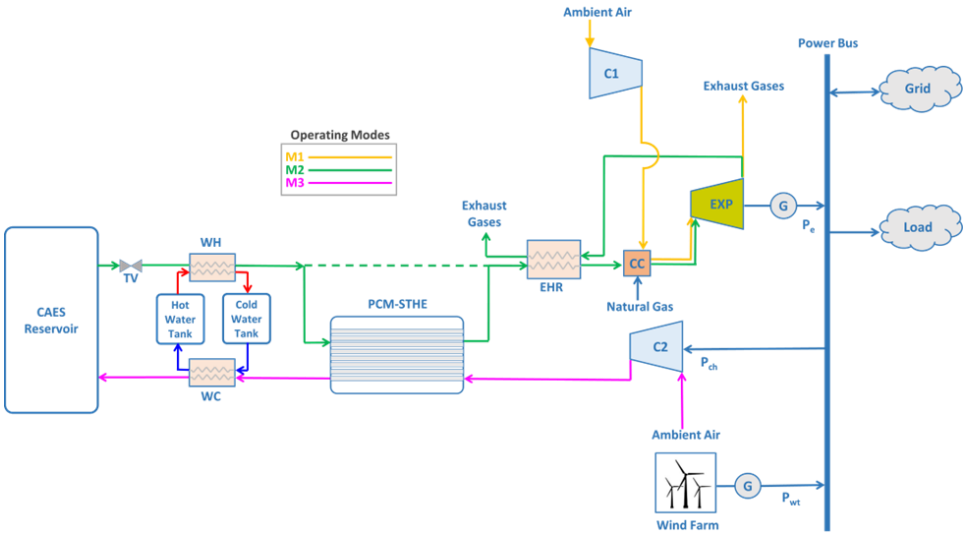

Fig. 1. Configuration 1 Block Diagram – Combined CAES-LHS Systems Coupled to a Gas Turbine

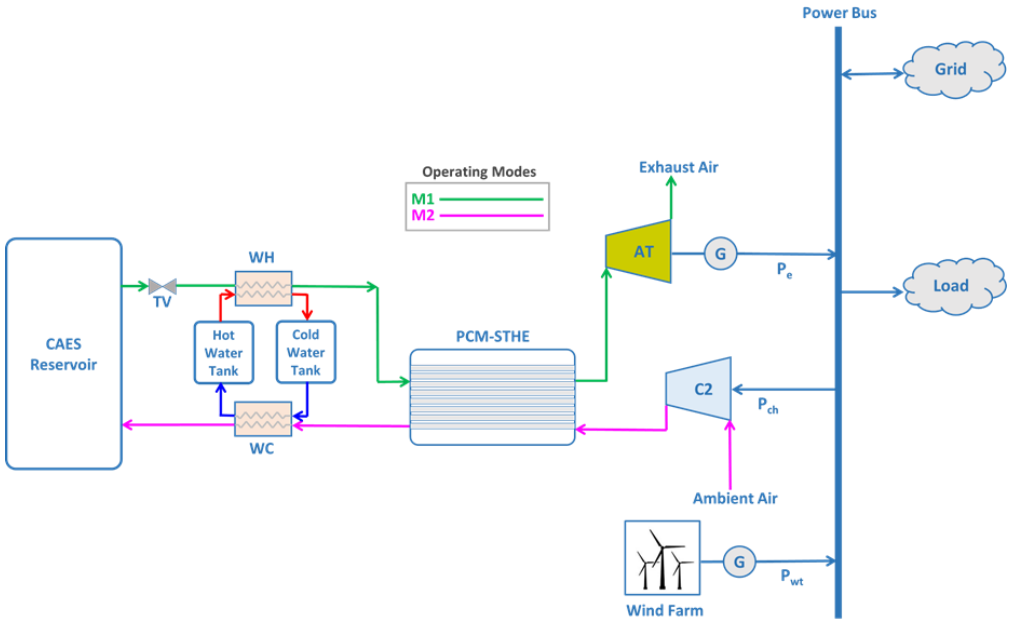

Fig. 2. Configuration 2 Block Diagram – Combined CAES-LHS Systems Coupled to an Air Turbine

compressed air is released from the CAES system into the gas turbine at a constant pressure (via the throttling valve TV). The temperaC1ture of the released compressed air is much lower than the temperature that would normally be expected at the inlet of a gas turbine's combustion chamber. Consequently, the compressed air will have to be preheated by initially passing it through a water-based preheater (WH), then through the PCM-based STHE, then into the EHR, before entering the combustion chamber CC. The hot gases produced in the CC expand in the gas turbine expander (EXP), which in turn drives the generator (G) to produce electrical power P_e. The heat stored in the PCM is discharged into the compressed air stream, and the PCM starts solidifying. In case the PCM is completely solidified before the end of the air discharge period, the STHE will be bypassed, and the compressed air stream will be directly fed into the EHR system for the remaining duration of the discharge operation.

After the system was operated in mode M2 for a certain time period, both the A-CAES and PCM-based LHS systems will need to be subsequently recharged, under mode M3 (charging mode). In this mode, an auxiliary compressor C2 is energized using excess off-peak grid electricity or renewable energy from the wind farm (P_{wt}), in order to produce compressed air to be stored in the CAES system. The produced compressed air flows through the PCM-based STHE where its heat is extracted by the PCM which starts melting. Before entering the CAES reservoir, the compressed air at the outlet of the STHE (which is still at a relatively high temperature) is passed through a water-based cooler (WC) where its heat is further extracted and stored for later use during the discharge operation. Another configuration of the power system was also investigated, in which the GT is replaced by an AT, as shown in the block diagram of Figure 2. This configuration can operate in 2 modes. In Mode M1 (Discharge mode), the compressed air released from the CAES reservoir at a constant pressure (via the throttling valve TV) is preheated through the water-based preheater (WH), then into the PCM-based STHE, before expanding in the AT to generate electrical power P_e through G. The charging mode (Mode M2)

of the air turbine configuration is the same as the charging mode M3 of the GT configuration.

2.2 Modeling Assumptions

The compressed air flowing through or stored within all system components was modelled as an ideal gas, and the ambient temperature and atmospheric pressure were assumed to be 298 K and 1.013 bar, respectively. During the charging operation, the compressed air temperature at the STHE inlet should be higher than the melting point of the PCM. Furthermore, the air temperature needed at the beginning of the charging operation will always be dictated by the initial pressure in the CAES reservoir. This is due to the fact that the charging compression train C2 needs to overcome the increasing pressure building up in the CAES reservoir during the filling (charging) process. The resulting pressure at the outlet of the last compression stage in C2 would therefore determine the charging temperature of the compressed air produced. As a conservative approach, this temperature should match the melting point of the PCM at the beginning of the charging operation. This temperature will gradually increase as the pressure builds up in the CAES reservoir. The European Association for Storage of Energy (EASE) reports that compressor discharge temperatures in A-CAES systems can exceed 873 K (European Association for Storage of Energy (EASE), 2016), but the available technical literature lacks sufficient details on how much higher this temperature can be, given the current compressor technologies.

Throughout the simulation of the combined CAES-LHS systems, the PCM is kept in phase change mode, because the intent is to explore the contribution of PCM latent heat to the system performance. In other words, the behavior of the system under sensible heat transfer between the PCM and the compressed air is not investigated in this work. As for the charging/discharging operational constraints, it is assumed that a discharge operation of the combined CAES-LHS systems cannot be followed by another discharge operation. Once discharged, the storage system's state of charge is considered "empty", and the system is ready to be charged again. In other words, once the PCM is completely solidified, it will not be further discharged in sensible heat transfer mode. Also, the compressed air discharged from the reservoir is throttled at a pressure almost equal to the inlet pressure of the turbine, so the lowest permissible pressure in the reservoir cannot dip below this throttling setpoint.

The compressors and turbines are assumed to operate at constant isentropic efficiencies. In this study, the gas and air turbines are configured to operate at their design points by imposing fixed nominal pressure ratios (through throttling) and maintaining near-nominal mass flow rates. As a result, the assumption of constant isentropic efficiency is considered reasonable within the scope of the present analysis.

It is assumed that the final state of the combined CAES-LHS systems at the end of the discharge operation should correspond to their initial state at the beginning of charging. Once the charging operation is initiated, it should bring back the CAES system to its initial conditions (in terms of mass, temperature and pressure) and the LHS system to its initial 100% liquid fraction, in preparation for any upcoming discharge operation. For example, if the CAES reservoir at the beginning of the discharge operation is at 450 K and 44 bar, and it is discharged to 350 K and 17 bar, then it should be brought back to its initial state of 450 K and 44 bar at the end of the charging operation. Similarly, the quantity of air fed into the CAES reservoir in charging mode should be equal to the quantity of air released from the CAES reservoir in discharge mode.

Various charging durations were evaluated to take advantage of the variability in wind energy for charging the system. Specifically, charging durations ranging between 2 and 10 hours were attempted in the simulation calculations, whereas the discharge operation was fixed for 2 hours. With regards to the renewable energy source, it is assumed that the integrated power system is operating under ideal wind conditions whereby excess wind power is continuously available to charge the combined A-CAES and PCM-based LHS systems. For example, under ideal wind conditions, a 4-hour charging period would be immediately followed by a 2-hour discharge operation, after which the cycle would repeat with another 4-hour charging period, and so on. In other words, wind power is always readily available to carry out a charging operation immediately after a discharge operation.

2.3 Analytical Modeling of System Components

Simulating the operation of the power system was conducted by using analytical models of its various components, instead of resorting to resource-intensive computational fluid dynamics (CFD) simulations. In fact, the analytical models would enable the timely prediction of the temperature and pressure profiles inside the CAES reservoir, the phase change fraction evolution of the PCM in the STHE, as well as the transient temperature profiles of the compressed air at the inlets and outlets of the various system components, all during charging and discharging modes, without the need for lengthy CFD simulations. The analytical models that were applied in simulating the operation of the overall system are not presented in this paper for the sake of brevity. Instead, a general description of how they were formulated is provided.

The operation of the gas and air turbines, the charging compression train C2 and the air-preheater (WH) and air cooler (WC), was modelled using the thermodynamic analyses adopted in (Moran *et al.*, 2020), while the plate-fin regenerator (EHR component) was modelled in accordance with the approach in (Kays & London, 2018).

The modeling of the PCM-based STHE during charging and discharge modes was based on the analytical model proposed and validated through Ansys® Fluent® CFD simulations in (Karam *et al.*, 2025). The PCM-based storage heat exchanger was modeled by considering a phase change front that propagates radially toward the tube center during melting and solidification of the PCM inside the tubes. Heat transfer within the PCM was assumed to occur by conduction and the evolution of the transient thermal resistance was evaluated dynamically at each time step of the analytical model simulation. This time-varying internal resistance was then incorporated into the heat transfer formulation which was based on the ε-NTU method. The analytical model was able to consistently predict the PCM liquid/solid fraction evolution with a Root Mean Square Error less than 5%, and the compressed air temperature at the STHE outlet with a Mean Absolute Percentage Error less than 3%, for PCM Stefan numbers less than 2, without the need to resort to computationally-demanding CFD simulations.

The dynamic behavior of the compressed air reservoir was modelled in accordance with (Karam, 2025) where the evolution of the compressed air temperature and pressure inside the CAES reservoir (during charging and discharge modes) and the discharged air temperature are accurately predicted. As for the compressed air (and exhaust gases) thermophysical properties,

these were evaluated using analytical expressions resulting from polynomial regression conducted on thermodynamics data tabulated in (Moran *et al.*, 2020) and (Kays & London, 2018). These analytical expressions make the evaluation of the compressed air properties more convenient when incorporated into a programmable analytical model, eliminating the need to resort to graphs or tabulated data throughout the iterative calculation process.

Since the integration of the combined storage systems into the GT configuration is expected to result in a reduction in fuel consumption, it would be relevant to evaluate the fuel-saving efficiency η_{fs} by relating the saved fuel energy to the input charging energy (responsible for this fuel reduction), as expressed in Equation 1:

$$\eta_f = \frac{(\dot{m}_{f,av,std} - \dot{m}_{f,av,disch}) \times t_{disch} \times LHV_f}{E_{ch}} \times \left(\frac{1000}{3600}\right) \quad (1)$$

where $\dot{\mathbf{m}}_{\mathbf{f,av,disch}}$ is the average fuel consumption rate during the 2-hour discharge period (in ton/h), $\dot{\mathbf{m}}_{\mathbf{f,av,std}}$ is the fuel consumption of the GT when operating in standalone mode, $\mathbf{E_{ch}}$ is the input charging energy (in MWh) and $\mathbf{t_{disch}}$ corresponds to the 2-hour discharge duration (in hours). A Lower Heating Value ($\mathbf{LHV_f}$) of 47.1 MJ/kg was adopted for natural gas (The Engineering Toolbox, 2025b).

The thermodynamic performance of the combined storage systems is investigated in this study by evaluating and comparing the exergetic roundtrip efficiencies in the GT and AT configurations.

For the GT configuration, the exergetic roundtrip efficiency $\boldsymbol{\eta_{ex,GT}}$ was evaluated using Equation 2:

$$\boldsymbol{\eta_{ex,GT}} = \frac{\boldsymbol{P_{GT} \times t_{disch}}}{\left(\frac{1000}{3600}\right) \times \frac{\dot{m}_{f,av,disch} \times t_{disch} \times \bar{e}^{ch}_{CH4}}{M_{CH4}} + (\dot{E}x_{C2} \times t_{ch})} \quad (2)$$

where $\mathbf{P_{GT}}$ represents the steady GT output (in MW) produced during the 2-hour discharge duration $\mathbf{t_{disch}}$ (in hours), $\dot{\mathbf{m}}_{\mathbf{f,av,disch}}$ the average fuel consumption rate during the discharge operation (in ton/h), $\bar{\mathbf{e}}^{\mathbf{ch}}_{\mathbf{CH4}}$ the standard molar chemical exergy for CH_4 at ambient temperature and pressure, taken as 831.65 MJ/kmol (Moran *et al.*, 2020), and $\dot{\mathbf{E}}\mathbf{x}_{\mathbf{C2}}$ the average input exergy rate at the compression train C2 (in MW) during the charging duration $\mathbf{t_{ch}}$ (in hours). $\dot{\mathbf{E}}\mathbf{x}_{\mathbf{C2}}$ corresponds to the average electric input power $\mathbf{P_{av,ch}}$ consumed during the charging operation. $\mathbf{M_{CH4}}$ is the molar mass for CH_4 (16.04 kg/kmol).

The exergetic roundtrip efficiency in the AT configuration ($\eta_{ex,AT}$) was computed using:

$$\eta_{ex,AT} = \frac{P_{AT,av} \times t_{disch}}{\dot{E}x_{C2} \times t_{ch}} \quad (3)$$

where $\mathbf{P_{AT,av}}$ represents the average AT power output (in MW) throughout the 2-hour discharge duration $\mathbf{t_{disch}}$ (in hours), and $\dot{\mathbf{E}}\mathbf{x}_{\mathbf{C2}}$ the average input exergy rate at the compression train C2 (in MW) during the charging duration $\mathbf{t_{ch}}$ (in hours).

2.4 System Components Parameters & Physical Characteristics

The parameters and physical characteristics of the simulated system's individual components can be found in Appendix A. The PCM stored in the tubes of the STHE was chosen to be K_2CO_3(34.5%)-Na_2CO_3(33.4%)-Li_2CO_3(32.1%), which belongs to the category of carbonates and which is known for its thermal stability (Liu *et al.*, 2017). Its thermophysical properties can be found in Appendix A. The cycling stability test of the selected PCM demonstrated that it can reach 1000 thermal cycles (Milian *et al.*, 2020). Accordingly, every time the number of charging-discharging cycles reaches 1000 cycles, the quantity of PCM stored in the STHE's tubes is assumed to have reached the end of its service life and will therefore need to be replaced by a new batch. The number of yearly PCM replacements can therefore be assessed by dividing the expected number of yearly charging-discharging cycles by the PCM's thermal cycle limit of 1000 cycles. The market price reported by the US National Renewable Energy Laboratory (NREL) for the selected PCM is around 2.5 $/kg (Mehos *et al.*, 2017). But this value is an indicative reference that would need to be refined, as actual costs are subject to market variability. The STHE tubes' length varied based on the charging duration being implemented. The resulting lengths ranged between 4.3 m (for 2-hour charging) and 13.75 m (for 10-hour charging).

The compression train C2 needed to produce the charging compressed air is assumed to be made of 4 stages, without any intercoolers. Resorting to intercoolers would not be useful in such an application, because the aim is to attain an elevated compressed air temperature, capable of melting the high-temperature PCM. The same compression ratio was applied across all stages, with each stage assumed to be operating at an isentropic efficiency of 85% and an electro-mechanical efficiency of 98%. With regards to the water-based air cooler (WC), a constant 75% heat transfer effectiveness was assumed for simplification purposes while the entering water temperature was fixed at 298 K. As for the water-based air preheater (WH), a constant 75% heat transfer effectiveness was also adopted while the entering water temperature was fixed at 333 K.

The CAES system was assumed to be an existing underground reservoir with a fixed volume of 19,424 m^3 and an initial compressed air temperature of 353 K at the beginning of the charging operation. The simulation of the integrated power system during charging and discharging modes was carried out by linking the various analytical models of the individual system components and solving the simultaneous set of equations of these models, during each time step of the charging/discharging operation. The General Algebraic Modeling Software (GAMS) was used to perform the stepwise transient computations (GAMS Development Corp./GAMS Software GmbH, 2024)

3. Simulation Results & Discussion

3.1 Simulation Results of the Gas Turbine Configuration

In this part, the performance of the combined storage systems was explored when coupled to the gas turbine (configuration 1). During the charging operation, the compressed air at the outlet of C2 should be at a temperature higher than the PCM melting point (670 K). Therefore, the produced compressed air temperature at the beginning of the charging operation should be slightly higher than 670 K. This temperature corresponds to a pressure of 17.69 bar at the outlet of the last compression stage, which in turn corresponds to the initial pressure expected in the CAES reservoir. As the compression train continues to fill the reservoir, the pressure and the temperature of the compressed air progressively increase throughout the charging period. This increasingly hotter air will continue to melt the PCM until it becomes 100% liquid, marking the end of the charging operation. The simulation calculations were conducted for charging durations

Table 1
Compression Train C2 Simulation Results

Compression Train Variables	Charging Scenario								
	2-hour	3-hour	4-hour	5-hour	6-hour	7-hour	8-hour	9-hour	10-hour
$\dot{m}_{air,ch}$ (Kg/s)	45.0	30.0	22.50	18.0	15.0	12.86	11.25	10.0	9.0
Max. Compression Ratio (per stage)	2.583	2.579	2.577	2.576	2.575	2.574	2.573	2.573	2.572
$P_{av,ch}$(MW)	22.98	15.30	11.46	9.17	7.64	6.54	5.73	5.09	4.58
E_{ch}(MWh)	45.965	45.910	45.879	45.858	45.845	45.836	45.828	45.822	45.818
T_{ch} Range (K)	670-868	670-867	670-866	670-865	670-865	670-865	670-864	670-864	670-864

ranging between 2 and 10 hours. During the 2-hour discharge of the combined CAES-LHS systems, the throttled air exiting the CAES reservoir is initially preheated in WH using the thermal energy stored in water during the charging phase. Subsequently, it flows into the PCM-based STHE, then through the EHR for additional preheating. The evolution of the PCM solid fraction within the STHE and the PCM solidification time are continuously monitored; when complete solidification is reached, the air stream bypasses the STHE and flows directly into the EHR for the remaining duration of the discharge operation. The average gas consumption of the turbine is also calculated on an hourly basis throughout the 2-hour discharge period.

Key performance indicators of the combined CAES-LHS systems such as the required charging power, fuel savings, avoided CO_2 emissions, fuel-saving efficiency and exergetic roundtrip efficiencies were all evaluated (from the simulation results) under ideal wind conditions.

3.1.1 Compression Train C2 Results

Error! Reference source not found. presents the simulation results of compression train C2 for each charging scenario. The charging mass flow rate ($\dot{m}_{air,ch}$) ensures that the amount of air filling the CAES reservoir during each charging duration is equal to the quantity of air that will be released from the reservoir during the 2-hour discharge operation. The highest temperature reached at the outlet of the last compression stage (T_{ch}) across all scenarios corresponds to the 2-hour charging scenario (868 K). This value falls within the limits of compressor discharge temperatures reported by EASE for A-CAES systems. A major outcome of the simulation results is the average hourly input charging power ($P_{av,ch}$) consumed by compression train C2 for all charging scenarios. As can be noticed, shorter charging durations are associated with significantly higher power demands, resulting in steeper charging profiles. This may pose challenges when using intermittent renewable resources such as wind, whose power output does not typically vary rapidly. On the other hand, longer charging durations yield smoother and more stable power profiles, which may be operationally advantageous because they align better with the gradual fluctuations of wind power. But the operational benefit of smoother charging must be weighed against its economic impact. Extending the charging time reduces the frequency of charging-discharging cycles per year, which may limit the opportunities to reduce natural gas consumption. As for the energy needed to charge the combined CAES-LHS systems (E_{ch}), it can noticed from the values reported in Error! Reference source not found. that it remains nearly constant across all scenarios. This is due to the fact that, in each charging scenario, the CAES reservoir starts and ends at the same temperature and pressure conditions, while the PCM is being charged in the STHE.

Figure 3 shows the evolution of the PCM liquid fraction with the temperature and pressure profiles at the outlet of the last compression stage of C2, for the 4-hour charging scenario presented here as an example case. As shown in Fig. 3a, the progressive increase in the compressor discharge temperature

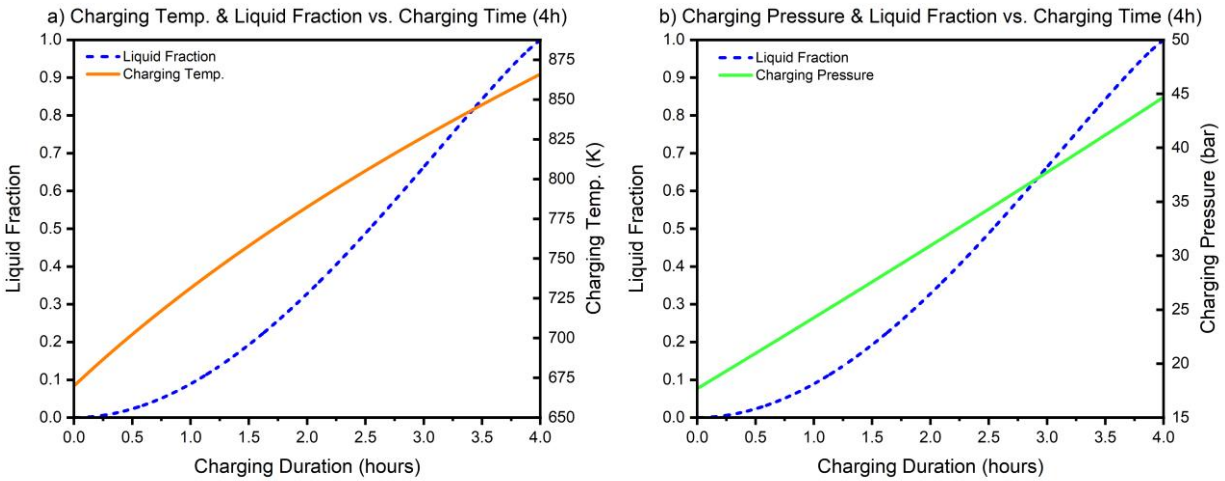

Fig. 3. Charging Temperature, Pressure & Liquid Fraction Evolution (4-h Charging)

Table 2
CAES Reservoir Simulation Results

CAES Reservoir Variables	Charging Scenario								
	2-hour	3-hour	4-hour	5-hour	6-hour	7-hour	8-hour	9-hour	10-hour
Temperature range CHARGING (K)	353-460	353-458	353-456	353-455	353-454	353-454	353-453	353-453	353-453
Pressure range CHARGING (bar)	17.69-45.10	17.69-44.85	17.69-44.70	17.69-44.59	17.69-44.52	17.69-44.47	17.69-44.43	17.69-44.39	17.69-44.37
Temperature range DISCHARGE (K)	460-358	458-356	456-355	455-354	454-353	454-353	453-352	453-352	453-352
Pressure range DISCHARGE (bar)	45.10-18.28	44.85-18.18	44.70-18.12	44.59-18.07	44.52-18.04	44.47-18.02	44.43-18.00	44.39-17.99	44.37-17.97

provides the thermal potential required for melting the PCM in the STHE, resulting in a gradual and almost monotonic rise of the liquid fraction. By the end of this 4-hour charging period, the PCM within the STHE is fully melted, marking the completion of the charging operation. In parallel, Fig. 3b shows a steady increase in the charging pressure, reflecting the continuous filling of the CAES reservoir at a controlled mass flow rate. The simultaneous increase in charging pressure and PCM liquid fraction shows the strong coupling between air compression, thermal energy transfer, and latent heat storage in the integrated CAES–LHS configuration.

3.1.2 CAES Reservoir Results

Table 2 shows the simulation results pertaining to the CAES reservoir which initially contains air at a temperature of 353 K and a pressure of 17.69 bar at the onset of the charging operation. This pressure value will ensure that compressed air is produced at a temperature of 670 K (PCM melting point) at the outlet of the last stage of C2 at the beginning of the charging operation. As can be seen from the table, the final air temperature and pressure in the CAES reservoir at the end of the 2-hour discharge operation almost correspond to those at the beginning of any charging scenario. Moreover, the range of air temperatures in the reservoir complies with the temperature levels expected in low-temperature adiabatic CAES systems (Salvini, 2018). The pressure building up in the CAES reservoir almost corresponds to the pressure at the last stage of C2, since the pressure drop in the STHE and WC turned out to be negligible. This can be verified by comparing the charging pressure in Figure 3 at the end of the charging operation (approx. 45 bar) with the final pressure value in the CAES reservoir in Table 2 for the 4-hour charging scenario (44.70 bar).

3.1.3 STHE Sizing Results & PCM Behavior

At the beginning of the charging operation, the PCM stored in the STHE is assumed to be in 100% solid phase at its solidus temperature. At the end of the charging process, the PCM will be completely melted. Both the charging mass flow rate of compressed air ($\dot{\mathbf{m}}_{\mathbf{air,ch}}$) and its corresponding temperature at the outlet of compressor C2 ($\mathbf{T_{ch}}$) play a key role in determining the PCM mass stored in the heat exchanger tubes ($\mathbf{m_{pcm}}$) that needs to be melted during a given charging duration. At a fixed tube diameter of 95.6 mm and tube count of 350, the STHE size will depend on the length of the tubes, which is expected to vary for each charging scenario. The sizing results for the PCM-based STHE are reported in Table 3.

During the 2-hour discharge operation, the solidification time increases across the different charging scenarios shown in Table 3, each of which corresponds to a distinct STHE size and PCM mass. This allows more effective utilization of the PCM's latent heat in reducing gas consumption. But these fuel savings will have to outweigh the additional cost associated with the larger STHE sizes. This trade-off will have to be examined in the context of an economic analysis to be performed in a future study.

3.1.4 Gas Consumption Results

As noted previously, the solidification time increases with the size of the STHE leading to a more effective use of the PCM latent heat in preheating the compressed air released from the CAES reservoir. The resulting average gas consumption rate ($\dot{\mathbf{m}}_{\mathbf{f,av,disch}}$) during the 2-hour discharge operation following a certain charging scenario, is reported in Table 4 for all charging durations. The simulation results for $\dot{\mathbf{m}}_{\mathbf{f,av,disch}}$ are less than the 2.578 ton/h fuel consumption of the gas turbine when operating in standalone mode ($\dot{\mathbf{m}}_{\mathbf{f,av,std}}$). The reduction in fuel consumption rate resulting from the implementation of the combined CAES-LHS storage systems varied between 43.52% and 44.91% depending on the charging scenario adopted. This reduction emphasizes the potential benefits that can be

Table 3
PCM-based STHE Simulation Results

STHE Variables	Charging Scenario								
	2-hour	3-hour	4-hour	5-hour	6-hour	7-hour	8-hour	9-hour	10-hour
Tube Length (m)	4.30	7.45	9.45	11.0	11.75	12.50	13.0	13.50	13.75
$\mathbf{m_{pcm}}$ (ton)	24.85	43.05	54.61	63.56	67.90	72.23	75.12	78.01	79.45
Solidification time (minutes)	42	53	59	63	66	68	69	71	72

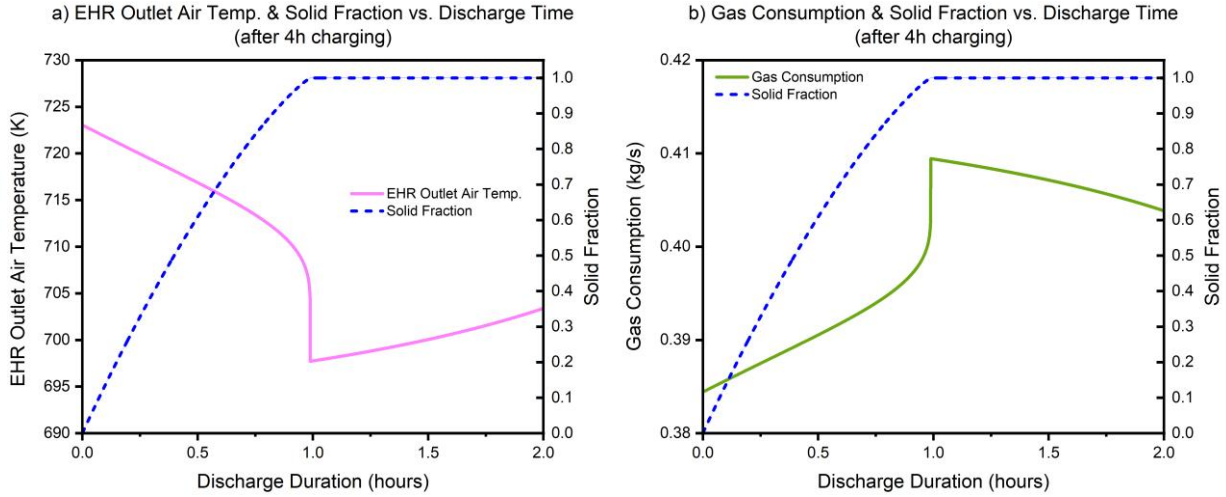

Fig. 4. Evolution of Solid Fraction, EHR Outlet Air Temp. & Gas Consumption (4-h Charging)

achieved from coupling the combined CAES and PCM-based LHS systems to a gas turbine.

Figure 4 shows how the gas consumption (in kg/s) and the compressed air temperature (in K) at the inlet of the turbine's combustion chamber (i.e. EHR outlet) vary with the PCM solid fraction during the 2-hour discharge operation following the 4-hour charging scenario (used here as an illustrative case). At the start of the discharge operation, the compressed air at the EHR outlet is preheated to temperatures as high as 723 K. As the PCM solidifies, the preheated air temperature gradually declines until the PCM is fully solidified, at which point the air stream bypasses the STHE and flows only through the EHR system. This transition is marked by a sharp drop in air temperature, clearly indicating the end of latent heat contribution. A similar trend is observed in the gas consumption curve, where a noticeable increase occurs once the PCM is fully solidified. This emphasizes the key role that latent heat plays in enhancing thermal efficiency and reducing fuel consumption during discharge operations.

The avoided CO_2 emissions (in tons/year) resulting from the implementation of the combined CAES-LHS systems in the GT configuration are summarized in Table 5, for each charging scenario. In this table, the number of yearly charging/discharging cycles was determined based on ideal wind conditions whereby excess wind power is continuously available to charge the storage system. Based on these charging/discharging cycles, the annual fuel savings were then quantified using the gas consumption rates of the turbine in discharge mode ($\dot{m}_{f,av,disch}$) and in standalone mode while the storage system is being charged ($\dot{m}_{f,av,std}$), both reported earlier in Table 4.. The avoided CO_2 emissions were subsequently derived from these fuel savings using an emission factor of 2.75 kg CO_2 per kg of natural gas burnt (The Engineering Toolbox, 2025a).

Table 4
Gas Turbine Fuel Consumption Rate in Standalone & Discharge Modes

GT Variables	Charging Scenario								
	2-hour	**3-hour**	**4-hour**	**5-hour**	**6-hour**	**7-hour**	**8-hour**	**9-hour**	**10-hour**
$\dot{m}_{f,av,disch}$ (ton/h)	1.456	1.444	1.437	1.431	1.428	1.425	1.423	1.421	1.420
$\dot{m}_{f,av,std}$ (ton/h)	2.578	2.578	2.578	2.578	2.578	2.578	2.578	2.578	2.578
% Gas Consumption Rate Reduction	43.52%	43.99%	44.28%	44.51%	44.61%	44.72%	44.80%	44.87%	44.91%

Table 5
Yearly Fuel Savings & Avoided CO_2 Emissions Under Ideal Wind Conditions

GT Performance Metrics	Charging Scenario								
	2-hour	**3-hour**	**4-hour**	**5-hour**	**6-hour**	**7-hour**	**8-hour**	**9-hour**	**10-hour**
Yearly Charging/Discharging Cycles	2,190	1,752	1,460	1,251	1,095	973	876	796	730
Fuel Savings (ton/year)	4,916	3,974	3,334	2,872	2,519	2,245	2,024	1,843	1,691
Avoided CO_2 Emissions (ton/year)	13,518	10,929	9,168	7,899	6,928	6,174	5,565	5,068	4,649

Table 5 reveals a clear trade-off between charging duration and the magnitude of avoided CO_2 emissions. Shorter charging scenarios result in a higher number of annual charging–discharging cycles, which translates into larger yearly fuel savings and greater emissions reductions. Conversely, as the charging duration increases, the number of achievable annual cycles progressively decreases, leading to a corresponding reduction in fuel savings and avoided emissions. Although longer charging scenarios yield lower annual CO_2 mitigation, they offer operational advantages in terms of smoother power profiles and improved compatibility with variable wind resources. This highlights an inherent compromise between maximizing environmental benefits and ensuring operational feasibility and grid integration.

The proposed combined A-CAES and PCM-LHS systems hold promising potential with regards to avoided CO_2 emissions. For instance, implementing the 4-hour charging scenario is expected to reduce CO_2 emissions by 9,168 metric tons per year. According to the Greenhouse Gas Equivalencies calculator of the US Environment Protection Agency, this avoided CO_2 quantity is equivalent to greenhouse gas emissions from 2,138 gasoline-powered passenger vehicles driven for one year, or to CO_2 emissions from 1,231 homes energy use for one year, or to the amount of carbon sequestered by 9,196 acres of U.S. forests in one year (US Environment Protection Agency (EPA), 2025).

3.2 Simulation Results of the Air Turbine Configuration

In this part, the performance of the combined CAES-LHS systems was explored when coupled to an air turbine (configuration 2). It is assumed that the CAES and LHS systems have the same sizes adopted when coupled to the gas turbine, for the sake of consistency and fair comparison. Accordingly, the results previously presented for compressor C2, the PCM-STHE and the CAES reservoir during the various charging scenarios of the GT configuration apply to the AT configuration.

The compressed air mass flow rate in the air turbine is fixed at 44.5 kg/s, which is the rated exhaust mass flow rate of the 14.3-MW gas turbine. This mass flow rate ensures that the discharge operation through the air turbine lasts for 2 hours, bringing both the CAES reservoir and the STHE to the same final conditions obtained in the gas turbine configuration (in terms of temperature, pressure, and PCM phase fraction). In addition, the air turbine generator is assumed to operate with the same electro-mechanical and isentropic efficiencies as the gas turbine generator.

The throttled compressed air released from the CAES reservoir initially passes through the water-based air preheater (WH), then into the PCM-based STHE for further preheating, before driving the air turbine. Obviously, this setup does not include an exhaust heat recovery system. It is expected that the air temperature at the AT inlet will decrease as the PCM solidifies. This will decrease the power output of the AT which is more sensitive to inlet temperature than the GT. After complete PCM solidification and due to the lack of additional thermal input (such as that provided by the EHR in the GT configuration), the AT power output is significantly reduced.

Figure 5 shows an example case of how the AT electrical power output (in MW) and the compressed air temperature at its inlet vary with the PCM solid fraction evolution during the 2-hour discharge process, for the STHE size corresponding to the 4-hour charging scenario. At the start of the discharge operation, the compressed air is preheated to around 425 K. As the PCM starts solidifying, the preheated air temperature gradually declines until the PCM is fully solidified. At the same time, the turbine's power output gradually decreases from 8.6 MW to 6.17 MW within almost an hour. When the PCM is fully solidified, the air stream bypasses the STHE. This transition is manifested by a sudden drop in air temperature and power output. From this point onward, the compressed air is only preheated by the stream from the water-based preheater.

The gradual solidification of the PCM reflects the controlled release of stored thermal energy, which smooths the decline in both turbine inlet temperature and power output. Once the latent heat storage is depleted, a sharp reduction in AT power generation is observed. This illustrates how the duration of effective PCM utilization directly influences the quality of thermal integration and the overall performance of the discharge process.

3.3 Energetic Performance Comparison: GT vs. AT Configurations

3.3.1 Air Turbine Output Power

Although the setup of the combined CAES-LHS systems with the AT is fuel-independent, it has limited performance when compared to the GT configuration. Without the stabilizing thermal effect of the EHR, the air turbine performance is significantly degraded after PCM solidification, as was

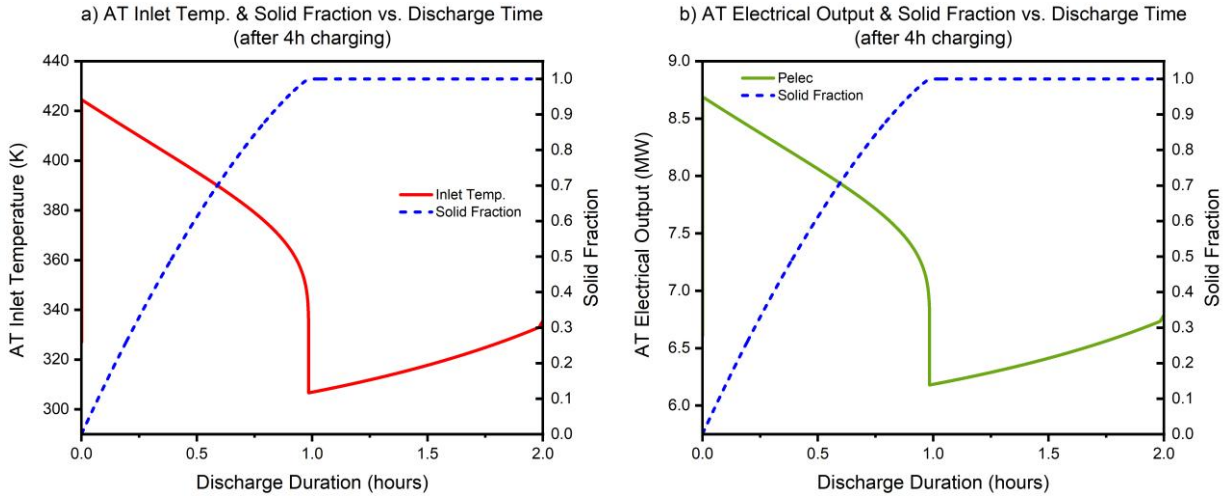

Fig. 5. Evolution of Solid Fraction, AT Inlet Temperature & Power Output (4-h Charging)

illustrated in part b of Figure 5. Table 6 summarizes the variation in average power output of the air turbine ($\mathbf{P_{AT,av}}$) across different charging scenarios and shows that it is 46% to 53% lower than the steady 14.3 MW output of the gas turbine ($\mathbf{P_{GT}}$).

The inability to maintain a stable and high turbine inlet temperature during discharge limits the system's capability to deliver firm power over extended periods. Increasing the charging duration yields only modest gains in recovered energy and does not significantly improve the dispatchable power capacity. The absence of active thermal regulation via the EHR leads to a progressive mismatch between the air temperature at turbine inlet and the optimal expansion requirements, once PCM solidification is completed. This highlights the stronger dependence of the AT configuration on the availability of stored thermal energy to maintain acceptable operating conditions, relative to the GT-based configuration.

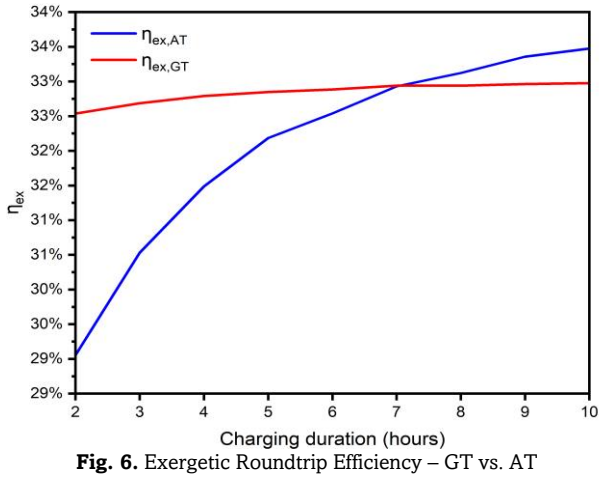

Fig. 6. Exergetic Roundtrip Efficiency – GT vs. AT Configuration

3.3.2 Gas Turbine Fuel-Saving Efficiency

As previously reported in Table 4, the implementation of the combined storage systems into the GT configuration resulted in a reduction in fuel consumption ranging between 43.52% and 44.91% depending on the charging scenario adopted. The corresponding fuel-saving efficiencies for the GT configuration for all the charging scenarios vary between 63.8% and 66.1%, as shown in Table 7.

The fuel-saving efficiency tends to increase with the charging duration as the gas consumption decreases due to the relatively longer solidification time of the PCM. Moreover, it would appear that these fuel-saving efficiencies compare favorably with performance metrics reported in the literature for other A-CAES setups. For example, they align well with the estimated 61.5% efficiency of an A-CAES system integrated with a cascaded packed bed thermal energy storage unit employing encapsulated PCM's (Bashiri Mousavi *et al.*, 2021), and with the estimated 76.2% efficiency achieved in an advanced trigenerative CAES system (Jiang *et al.*, 2019).

3.4. Exergetic Roundtrip Efficiency: GT vs. AT Configurations

The exergetic roundtrip efficiencies for the gas and air turbine configurations for all the charging scenarios are plotted in Figure 6. As can be seen, the exergetic roundtrip efficiency of the integrated power system is slightly higher in the GT configuration for charging durations shorter than 7 hours. Although this improvement is modest, it is important to recall that calculating $\eta_{ex,AT}$ was carried out under the assumption that the AT is operated at a constant air mass flow rate of 44.5 kg/s, enabling the same 2-hour discharge duration of the CAES-LHS systems in both GT and AT configurations. However, if the AT was required to deliver the same power output as the GT (14.3 MW) throughout the 2-hour discharge period, the mass flow rate of the compressed air released from the CAES reservoir would need to be increased to compensate for the decreasing temperature at the inlet of the air turbine; this would further accelerate both the solidification of the PCM and the depletion of the CAES reservoir, leading to a shorter discharge duration, and, consequently, an even lower roundtrip efficiency in the AT configuration.

For charging durations beyond 7 hours, the exergetic roundtrip efficiency in the AT configuration surpasses that of the GT configuration, making the AT setup more appealing for such charging durations. These results indicate that the selection between GT and AT configurations is strongly connected to the characteristics of the renewable energy source driving the charging process. In applications dominated by highly variable wind power, shorter charging periods may favor the GT configuration due to its ability to sustain turbine inlet conditions through fuel-assisted reheating. Conversely, renewable-dominated power systems characterized by longer and more stable charging intervals benefit from AT-based configurations. It is important to emphasize that these numerical values are specific to the particular power system being examined in this paper. Different findings would be expected if the parameters of the individual system components were changed.

While a comprehensive exergetic destruction analysis could provide insight into the relative contribution of each component

Table 6
GT & AT Power Output for All Charging Scenarios of the CAES-LHS systems

Turbines' Power Output	Charging Scenario								
	2-hour	3-hour	4-hour	5-hour	6-hour	7-hour	8-hour	9-hour	10-hour
$\mathbf{P_{GT}}$ (MW)	14.3	14.3	14.3	14.3	14.3	14.3	14.3	14.3	14.3
$\mathbf{P_{AT,av}}$ (MW)	6.68	7.01	7.22	7.38	7.46	7.54	7.59	7.64	7.67
% Power Reduction	53.3%	51.0%	49.5%	48.4%	47.8%	47.3%	46.9%	46.6%	46.4%

Table 7
Fuel-Saving Efficiencies for All Charging Scenarios – GT Configuration

GT Fuel Saving Efficiency	Charging Scenario								
	2-hour	3-hour	4-hour	5-hour	6-hour	7-hour	8-hour	9-hour	10-hour
η_{fs}	63.88%	64.64%	65.16%	65.47%	65.65%	65.90%	65.94%	66.06%	66.12%

to the overall irreversibility of the proposed configurations, such a detailed analysis is beyond the scope of the present work. Nevertheless, it would be important to address the main sources of exergy destruction within the PCM-based STHE, as this component is expected to experience large temperature gradients between the compressed air and the PCM. In fact, the irreversibilities in the PCM-based STHE arise primarily from finite temperature heat transfer between the compressed air and the PCM, pressure drop in the compressed air stream, and internal entropy generation due to heat diffusion and phase change within the PCM.

Exergy destruction occurs when heat is exchanged between the compressed air and the PCM across a finite temperature difference. This temperature mismatch makes the heat transfer process irreversible. The larger the temperature difference between the compressed air and the PCM, the higher the associated entropy generation and exergy loss. Also, as compressed air flows through the shell of the STHE, viscous friction and turbulence cause a loss of pressure. This pressure drop represents a degradation of the mechanical energy of the air that cannot be recovered for useful work.

Although phase change in the PCM occurs at an approximately constant temperature, internal thermal gradients would still develop due to heat conduction and phase change front movement. These gradients lead to irreversible heat diffusion within the PCM material. As a result, part of the thermal energy transferred during melting is irreversibly degraded, contributing to exergy destruction in the PCM-based STHE. It is worth highlighting that the simulation results obtained in this study confirm the validity of the ideal gas assumption for compressed air and satisfy the Stefan number criterion required for the proper application of the STHE analytical model proposed and validated in (Karam *et al.*, 2025).

4. Conclusion & Future Work

This study highlights several key findings and insights regarding the performance of the integrated CAES–LHS systems. The latent heat released by the PCM plays a crucial role during the discharge operation, sustaining the air temperature at the gas turbine inlet and enhancing its thermal efficiency. However, as the PCM completely solidifies, the inlet temperature begins to drop drastically, leading to higher gas consumption. This underlines the importance of latent heat storage not only in improving overall system efficiency and reducing fuel use, but also in contributing to avoided CO_2 emissions associated with the saved fuel. Using PCM's with higher melting points would require elevated outlet pressures from the compression train to produce compressed air at temperatures high enough to melt the PCM, thereby increasing the input charging demand and necessitating greater wind power availability to maintain operation. Enhancing the effective thermal conductivity of the PCM (through the integration of fins or metallic foams) would reduce the heat transfer resistance and temperature gradients within the PCM during both charging and discharging. This would promote more effective extraction and recovery of the heat of compression, thereby leading to an increase in the exergetic roundtrip efficiency of the A-CAES system.

The results of the study indicated that the fuel-saving efficiency of the gas turbine configuration increased with longer charging durations, attaining values between 63.8% and 66.1% over the range of 2 to 10 hours. In parallel, the exergetic roundtrip efficiency remains superior in the gas turbine setup for charging durations below 7 hours. Beyond this limit, the air turbine configuration demonstrates higher exergetic roundtrip efficiency when coupled to the CAES–LHS systems. Ideal wind conditions were assumed in this research. A future study could incorporate more realistic wind variability, thereby enabling a more representative comparison of the system's performance metrics. Also, an economic analysis of the combined CAES-LHS systems could be conducted to evaluate key performance metrics such as installed cost, payback period and levelized cost of storage. The trade-off between the improved fuel savings achieved with larger STHE units and the higher capital cost of these STHE's could be investigated in such work.

Future studies could explore how incorporating temperature-dependent PCM thermophysical properties affects the thermal behavior of the LHS system. In the same context, these studies could also examine the long-term effects of PCM corrosivity and thermal stability on the reliability of the LHS system. This would help forecast the operational lifespan and maintenance requirements of the PCM-based storage system, especially under real-world operating scenarios. Off-design performance analysis of the compressors and turbines could represent an important topic for future work, particularly in CAES systems operating under highly variable renewable energy conditions. Maximizing the system's exergetic roundtrip efficiency could be subsequently pursued by identifying the components with relatively high exergy destruction and optimizing these components' physical and operational parameters.

In conclusion, while the simulation results and performance assessment presented in this study are theoretical and based on simplifying assumptions, the findings offered a reliable foundation for approximating the expected behavior of the combined CAES-LHS systems when deployed in power system applications alongside renewable energy sources.

Author Contributions: T.K.: Conceptualization, methodology, formal analysis, writing—original draft, C.M.; Conceptualization, methodology, Writing—review and editing, supervision, resources, project administration, E.A.; Supervision. All authors have read and agreed to the published version of the manuscript.

Funding: This research was funded by the Lebanese International University, Beirut, Lebanon.

Conflicts of Interest: The authors declare no conflict of interest.

References

Anagnostopoulos, A., Navarro, M. E., Stefanidou, M., Ding, Y., & Gaidajis, G. (2021). Red mud-molten salt composites for medium-high temperature thermal energy storage and waste heat recovery applications. *Journal of Hazardous Materials*, *413*, 125407. https://doi.org/10.1016/j.jhazmat.2021.125407

Bashiri Mousavi, S., Adib, M., Soltani, M., Razmi, A. R., & Nathwani, J. (2021). Transient thermodynamic modeling and economic analysis of an adiabatic compressed air energy storage (A-CAES) based on cascade packed bed thermal energy storage with encapsulated phase change materials. *Energy Conversion and Management*, *243*, 114379. https://doi.org/10.1016/j.enconman.2021.114379

Becattini, V., Geissbühler, L., Zanganeh, G., Haselbacher, A., & Steinfeld, A. (2018). Pilot-scale demonstration of advanced adiabatic compressed air energy storage, Part 2: Tests with combined

sensible/latent thermal-energy storage. *Journal of Energy Storage*, *17*, 140–152. https://doi.org/https://doi.org/10.1016/j.est.2018.02.003

Bloch, M. (2021, January 25). *Compressed Air Energy Storage Project In SA Dumped*. Solarquotes Blog. https://www.solarquotes.com.au/blog/hydrostor-caes-strathalbyn-mb1852/

Burian, O., & Dančová, P. (2023). Compressed Air Energy Storage (CAES) and Liquid Air Energy Storage (LAES) Technologies—A Comparison Review of Technology Possibilities. *Processes*, *11*(11). https://doi.org/10.3390/pr11113061

COP28 UAE. (2023). *Compressed Air Energy Storage Revival of a Proven, Economical Solution for Long Duration Energy Storage*. https://www.cop28.com/en/schedule/compressed-air-energy-storage-revival-of-a-proven-economical-solution-for-long-duration-energy-st

European Association for Storage of Energy (EASE). (2016). *Adiabatic Compressed Air Energy Storage*. Energy Storage Technology Descriptions. https://ease-storage.eu/wp-content/uploads/2016/03/EASE_TD_ACAES.pdf

GAMS Development Corp./GAMS Software GmbH. (2024). *The General Algebraic Modeling System (GAMS)* (release 48.5.0 (December 20, 2024)). GAMS.

Geissbühler, L., Becattini, V., Zanganeh, G., Zavattoni, S., Barbato, M., Haselbacher, A., & Steinfeld, A. (2018). Pilot-scale demonstration of advanced adiabatic compressed air energy storage, Part 1: Plant description and tests with sensible thermal-energy storage. *Journal of Energy Storage*, *17*, 129–139. https://doi.org/https://doi.org/10.1016/j.est.2018.02.004

Ghorbani, B., Mehrpooya, M., & Ardehali, A. (2020). Energy and exergy analysis of wind farm integrated with compressed air energy storage using multi-stage phase change material. *Journal of Cleaner Production*, *259*, 120906. https://doi.org/10.1016/j.jclepro.2020.120906

Hydrostor. (2024). *Goderich Energy Storage Centre*. Hydrostor. https://hydrostor.ca/projects/the-goderich-a-caes-facility/

International Renewable Energy Agency. (2025). *Renewable Capacity Statistics 2025*. https://www.irena.org/-/media/Files/IRENA/Agency/Publication/2025/Mar/IRENA_DAT_RE_Capacity_Statistics_2025.pdf

International Renewable Energy Agency (IRENA). (2017). *Electricity Storage and Renewables: Costs and Markets to 2030*. www.irena.org/publications

Jafarizadeh, H., Soltani, M., & Nathwani, J. (2020). Assessment of the Huntorf compressed air energy storage plant performance under enhanced modifications. *Energy Conversion and Management*, *209*, 112662. https://doi.org/10.1016/j.enconman.2020.112662

Jiang, R., Yin, H., Peng, K., & Xu, Y. (2019). Multi-objective optimization, design and performance analysis of an advanced trigenerative micro compressed air energy storage system. *Energy Conversion and Management*, *186*, 323–333. https://doi.org/10.1016/j.enconman.2019.02.071

Karam, T. (2025). *Modeling & Performance Assessment of a Combined Adiabatic Compressed Air & Latent Heat Storage System Utilizing Phase Change Materials in a Renewable Energy Framework*. PhD thesis, Saint Joseph University of Beirut.

Karam, T., Maatouk, C., & Al Sarraf, E. (in press). Simplified Analytical Formulation for Thermal Behavior Prediction of a PCM-based Heat Storage System. *Contemporary Mathematics*.

Kays, W. M., & London, A. L. (2018). *Compact Heat Exchangers* (Third Edition). Scientific International Pvt. Ltd.

Khan, M. I., Asfand, F., & Al-Ghamdi, S. G. (2022). Progress in research and technological advancements of thermal energy storage systems for concentrated solar power. *Journal of Energy Storage*, *55*, 105860. https://doi.org/10.1016/j.est.2022.105860

Li, D., Hu, Y., Li, D., & Wang, J. (2019). Combined-cycle gas turbine power plant integration with cascaded latent heat thermal storage for fast dynamic responses. *Energy Conversion and Management*, *183*, 1–13. https://doi.org/10.1016/j.enconman.2018.12.082

Li, Q., Li, C., Du, Z., Jiang, F., & Ding, Y. (2019). A review of performance investigation and enhancement of shell and tube thermal energy storage device containing molten salt based phase change materials for medium and high temperature applications. *Applied Energy*, *255*, 113806. https://doi.org/https://doi.org/10.1016/j.apenergy.2019.113806

Li, R., Wang, H., & Zhang, H. (2019). Dynamic simulation of a cooling, heating and power system based on adiabatic compressed air energy storage. *Renewable Energy*, *138*, 326–339. https://doi.org/10.1016/j.renene.2019.01.086

Li, R., Zhang, Y., Chen, H., Zhang, H., Yang, Z., Yao, E., & Wang, H. (2021). Exploring thermodynamic potential of multiple phase change thermal energy storage for adiabatic compressed air energy storage system. *Journal of Energy Storage*, *33*, 102054. https://doi.org/10.1016/j.est.2020.102054

Liu, T. L., Liu, W. R., & Xu, X. H. (2017). Properties and heat transfer coefficients of four molten-salt high temperature heat transfer fluid candidates for concentrating solar power plants. *IOP Conference Series: Earth and Environmental Science*, *93*(1). https://doi.org/10.1088/1755-1315/93/1/012023

Mehos, M., Turchi, C., Gomez-Vidal, J., Wagner, M., Ma, Z., Ho, C., Kolb, W., Andraka, C., & Kruizenga, A. (2017). *Concentrating Solar Power Gen3 Demonstration Roadmap*. https://docs.nrel.gov/docs/fy17osti/67464.pdf

Milian, Y. E., Ushak, S., Cabeza, L. F., & Grageda, M. (2020). Advances in the development of latent heat storage materials based on inorganic lithium salts. *Solar Energy Materials and Solar Cells, 208*, 110344. https://doi.org/10.1016/j.solmat.2019.110344

Mofijur, M., Mahlia, T. M. I., Silitonga, A. S., Ong, H. C., Silakhori, M., Hasan, M. H., Putra, N., & Ashrafur Rahman, S. M. (2019). Phase change materials (PCM) for solar energy usages and storage: An overview. *Energies*, *12*(16). https://doi.org/10.3390/en12163167

Moran, M., Shapiro, H., Boettner, D., & Bailey, M. (2020). *Fundamentals of Engineering Thermodynamics* (9th Edition). Wiley.

Murray, C. (2024, April 10). World's largest' compressed air energy storage project connects to the grid in China. *Energy-Storage.News*. https://www.energy-storage.news/worlds-largest-compressed-air-energy-storage-project-connects-to-the-grid-in-china/

Peter Reinke. (2024). *Email Correspondence with HBI Haerter AG on RICAS2020 project*.

Prieto, C., & Cabeza, L. F. (2019). Thermal energy storage (TES) with phase change materials (PCM) in solar power plants (CSP). Concept and plant performance. *Applied Energy*, *254*, 113646. https://doi.org/10.1016/j.apenergy.2019.113646

Rabi, A. M., Radulovic, J., & Buick, J. M. (2023). Comprehensive Review of Compressed Air Energy Storage (CAES) Technologies. *Thermo*, *3*(1), 104–126. https://doi.org/10.3390/thermo3010008

REN21. (2024). *Renewables 2024 Global Status Report – Renewables In Energy Demand*. https://www.ren21.net/gsr-2024/

RICAS. (2020). *Design Study For The European Underground Research Infrastructure Related To Advanced Adiabatic Compressed Air Energy Storage*. RICAS. https://www.ricas2020.eu/project/project-objectives/design-concept/

Royo, P., Acevedo, L., Ferreira, V. J., García-Armingol, T., López-Sabirón, A. M., & Ferreira, G. (2019). High-temperature PCM-based thermal energy storage for industrial furnaces installed in energy-intensive industries. *Energy*, *173*, 1030–1040. https://doi.org/10.1016/j.energy.2019.02.118

Salvini, C. (2018). CAES systems integrated into a gas-steam combined plant: Design point performance assessment. *Energies*, *11*(2). https://doi.org/10.3390/en11020415

Shaw, V. (2024, May 16). World's largest compressed air energy storage project comes online in China. *Pv Magazine*. https://www.pv-magazine.com/2024/05/16/worlds-largest-compressed-air-energy-storage-project-comes-online-in-china/

Siemens Energy. (2025). *SGT-400 gas turbine*. https://www.siemens-energy.com/global/en/home/products-services/product/sgt-400.html#/

Tawalbeh, M., Khan, H. A., Al-Othman, A., Almomani, F., & Ajith, S. (2023). A comprehensive review on the recent advances in materials for thermal energy storage applications. *International Journal of Thermofluids*, *18*, 100326. https://doi.org/10.1016/j.ijft.2023.100326

Tehrani, S. S. M., Taylor, R. A., Saberi, P., & Diarce, G. (2016). Design and feasibility of high temperature shell and tube latent heat thermal energy storage system for solar thermal power plants.

Renewable Energy, *96*, 120–136. https://doi.org/10.1016/j.renene.2016.04.036

The Engineering Toolbox. (2025a). *Combustion of Fuels - Carbon Dioxide Emission*. https://www.engineeringtoolbox.com/co2-emission-fuels-d_1085.html

The Engineering Toolbox. (2025b). *Higher Calorific Values of Common Fuels: Reference & Data*. https://www.engineeringtoolbox.com/fuels-higher-calorific-values-d_169.html

US Environment Protection Agency (EPA). (2025). *Greenhouse Gas Equivalencies Calculator*. https://www.epa.gov/energy/greenhouse-gas-equivalencies-calculator

Wang, P., Zhao, P., Xu, W., Wang, J., & Dai, Y. (2019). Performance analysis of a combined heat and compressed air energy storage system with packed bed unit and electrical heater. *Applied Thermal Engineering*, *162*, 114321. https://doi.org/10.1016/j.applthermaleng.2019.114321

Wang, S., Zhang, X., Yang, L., Zhou, Y., & Wang, J. (2016). Experimental study of compressed air energy storage system with thermal energy storage. *Energy*, *103*, 182–191. https://doi.org/10.1016/j.energy.2016.02.125

Zhang, X., Gao, Z., Zhou, B., Guo, H., Xu, Y., Ding, Y., & Chen, H. (2024). Advanced Compressed Air Energy Storage Systems: Fundamentals and Applications. *Engineering*, *34*, 246–269. https://doi.org/10.1016/j.eng.2023.12.008

Zhou, Q., Du, D., Lu, C., He, Q., & Liu, W. (2019). A review of thermal energy storage in compressed air energy storage system. *Energy*, *188*, 115993. https://doi.org/10.1016/j.energy.2019.115993

Appendix A

Table A.1

Gas Turbine Parameters

Parameter	Value
Nominal Capacity	14.3 MW
Exhaust Temperature	802 K
Exhaust mass flow rate	44.5 kg/s
Electro-mechanical efficiency	98%
Compressor Isentropic Efficiency	85%
Compression Ratio	17

Table A.2
Plate-Fin Regenerator – General Parameters

Parameters	**Value**
Length × Width × Height	4 m × 1 m × 2 m
Plate thickness	0.3 mm
Fin Thermal conductivity	20.08 W/m.K

Table A.2
Plate-Fin Regenerator – Air Side & Exhaust Side Surface Geometry Parameters

Surface Geometry Parameters	**Air Side**	**Exhaust Side**
Plate spacing	6.35 mm	6.35 mm
Hydraulic diameter	4.453 mm	3.08 mm
Fin thickness	0.152 mm	0.152 mm
Ratio of heat transfer area to volume between plates	840 m^2/m^3	1204 m^2/m^3
Ratio of total heat transfer area to total heat exchanger volume	401.05 m^2/m^3	574.84 m^2/m^3
Ratio of fin area to total area	0.64	0.756
Total frontal area	4 m^2	2 m^2
Ratio of free flow area to frontal area	0.446	0.442
Free flow area	1.784 m^2	0.884 m^2
Total heat transfer area	3,208.4 m^2	4,598.73 m^2

Table A.3
Shell-and-Tube Heat Exchanger Parameters

Parameters	Value
Tube Layout	Triangular
Tube Layout constant	0.87
Tube count calculation constant	0.93
Tube count	350
Tube length	*varies*
Tube thickness	0 mm
Tube diameter	95.6 mm
Tube pitch	119.5 mm
Shell (inside) diameter	2.44 m
Shell Equivalent diameter	69.1 mm
Tubes Clearance	23.9 mm
Baffle count	0

Table A.4
PCM9 Thermophysical Properties

PCM melting temperature	670 K
PCM density	2,300 kg/m^3
PCM Latent Heat	276 kJ/kg
PCM thermal conductivity	2.02 W/m.K